Synthesis, Characterization and Photocatalytic Studies of Novel $SrFe_{12}O_{19}/TiO_2/SiO_2$/GO nanocomposite

Majji Suneetha[1*], Gandham Hima Bindu[1*], Duppati Swapna[1,2], Chapa Ramya Kumari[1], Konathala Jyothi Priya[1], Ravi Santhi Goldina[1] and Sanasi Paul Douglas[1*]

1. Department of Engineering Chemistry, Andhra University College of Engineering, Andhra University (A), Visakhapatnam- 530003, Andhra Pradesh, INDIA
2. Dadi Institute of Engineering and Technology, Anakapalli – 531002, INDIA
*maheshhanisony@gmail.com; himabinduauce@gmail.com; spdfchem@andhrauniversity.edu.in

Abstract

Sol-gel and Hummers created magnetic $SrFe_{12}O_{19}/TiO_2/SiO_2$/GO as a nanocomposite photocatalyst with a high crystalline TiO_2 shell. X-ray diffraction (XRD), Fourier Transform Infrared Spectroscopy (FTIR), High-resolution transmission electron microscopy (HRTEM), Scanning electron microscopy (SEM), Ultraviolet-visible diffuse reflectance spectroscopy (UV-DRS) and Vibrating sample magnetometer (VSM) were utilized to analyze the composite particles produced.

The findings demonstrate that the $SrFe_{12}O_{19}/TiO_2/SiO_2$/GO composite particles that were formed, were made up of spherical nanoparticles with a diameter of roughly 30 nm with silica serving as covering and fence between GO, titania shells and several $SrFe_{12}O_{19}$ small particles with a diameter of around 20 nm serving as cores. It exhibits a band gap energy. The value is 2.29 eV. Under UV irradiation, the composite photocatalytic particle's photocatalytic activity was also examined for the breakdown of Rhodamine B and Methylene Blue under UV light, 100% of the dyes degrade in 60 and 70 minutes when magnetic composite nanoparticles were present. Using magnetic separation, the created magnetic composite nanoparticles showed significant photocatalytic efficiency and could be utilized for remediating contaminated water.

Keywords: $SrFe_{12}O_{19}/TiO_2/SiO_2$/GO, Sol-gel Method, Hummers Method, Photocatalytic Activity, Nanocomposite, Rhodamine B, Methylene Blue, Sol-gel Method, Hummers Method, Antibacterial activity.

Introduction

Among the industries that pollute the air, water and land, the industries producing produce textiles are more. In textile sector effluents, persistent organic pollutants (POPs) such as pigments and dyes are produced in large quantities and released 5–1500 mg L^{-1}. Significant quantities of these pollutants are also being released into wastewater by other industries, such as pulp, paper, leather, food and beverage production, pharmaceuticals and cosmetics[14]. As industrialization accelerates, various industries are discharging pollutants into the environment, resulting in significant health and environmental issues. In addition, the presence of these colors in water bodies will soon put aquatic life at risk[6].

The extensive use of dyes, mainly in a range of industrial activities like the development of photoelectrochemical cells, the assembly of light-harvesting arrays, the staining of wood, the coloring of hair, the formulation of cosmetics, the production of medications, the creation of color photography, the manufacturing and the tanning of leather and paper, significantly contributes to their eventual presence in wastewater[7]. The four most significant groups of dyes are anthraquinone, phthalocyanine, triaryl methane and azo. Azo dyes have extensive application in the textile sector. RhB is a common dye in industries and is a member of the xanthene dye class. It has remarkable brightness, outstanding stability and good water solubility. Additionally, several biological applications are suitable for it[17].

Rhodamine B is an organic and synthetic dye from the rhodamine family, distinguished by its xanthene core structure. Its chemical formula is $C_{28}H_{31}ClN_2O_3$ and it has a molecular weight of about 479.01 g/mol. The dye usually appears as a dark pink or red powder or solution and is soluble in water. Rhodamine B is extensively utilized as coloration in plastics, textiles and food products because of its vivid and durable color. Additionally, it serves as a tracer in studies of water flow and pollution due to its high visibility and distinctive. However, Rhodamine B poses potential health risks if inhaled. It is toxic to consume and it influences the skin, potentially causing irritation or allergic reactions. Its presence in wastewater and the environment raises concerns about its possible impact on aquatic life and ecosystems, leading to efforts to manage and reduce its environmental footprint through appropriate disposal and treatment practices[8].

Photocatalysis is recognized as one of the advanced oxidation processes. One of the more recent methods that uses photocatalysts to break down organic contaminants is photocatalytic degradation[1]. Ferrites are now considered adsorbents due to their magnetic properties and mechanical and chemical stability[9]. With a value of roughly 2.29 eV, M-type $SrFe_{12}O_{19}$ is considered an environmentally beneficial magnetic material that is an n-type semiconductor and has been used to break down a variety of synthetic organic dyes, including methyl orange, toluidine blue and MB[4]. $SrFe_{12}O_{19}$ also possesses several other noteworthy qualities such as

chemical stability, cost-effectiveness and permanent magnetism which are employed in various other industries including magnetic hyperthermia, microwave absorbers, corrosion resistors and recording media. $SrFe_{12}O_{19}$'s primary benefit is its ease of regaining and feasibility as a photocatalyst. The magnetic properties of $SrFe_{12}O_{19}$ make it easy to separate using an external magnetic field.

As a result, it is possible to extract the catalysts from the treated solution without releasing more pollutants[5]. Nanomaterials have proven to be effective in removing heavy metal ions, inorganic anions, dyes and microbes from water. These materials comprise of carbon nanotubes (CNTs), metal and metal oxide np's and various nanocomposite materials. Minerals, parent rocks, agriculture, sewage disposal, metallurgical processes and energy production are some of the heavy metal ions including lead, copper, zinc, cadmium, chromium, nickel, mercury and cobalt ions entering water systems through various means[10].

Our attention has been drawn to applying materials based on graphene oxide in heavy metal ions and dyes[2]. Magnetic properties of hexagonal ferrites can be altered by doping their surface. The study claims that graphene oxide is one of the appropriate carbon-based compounds for compositing with hexagonal ferrites because it is an efficient adsorbent for various pollutants[11]. This material has a high adsorption capacity, exhibits superparamagnetic, possesses a large surface area and a high surface-to-volume ratio and can be easily separated using external magnetic fields. Due to their enhanced capabilities, it has been discovered that the dispersion of magnetic nanoparticles over two-dimensional materials, including graphene sheets, may become a new area of study in the future. Consequently, their application shows considerable potential for an array of uses in biological domains, wastewater treatment and catalysis.

Graphene is a promising material consisting of a single layer of carbon atoms arranged in a 2D honeycomb structure, making it a strong contender for graphene-based composite nanomaterials due to its large surface area, flexibility, chemical stability and extremely high electrical conductivity[13]. Creating a brand-new hybrid photocatalyst consisting of magnetic strontium ferrite ($SrFe_{12}O_{19}$) and TiO_2-supported GO nanofibers, the photocatalyst ($GO/TiO_2/SrFe_{12}O_{19}/SiO_2$) may be magnetically retrieved and reused from an aqueous suspension. It can also capture solar photons in the UV and visible parts of the electromagnetic spectrum. By breaking down a hazardous and bio-recalcitrant insecticide under sunlight irradiation, the photocatalytic activity was studied[3].

SiO_2 interlayer was formed as a shell around the magnetic particles which could boost the photoactivity of the magnetic photocatalyst. The suppression of the e−/h+ recombination rate between ferrite–TiO_2 surfaces was identified as the cause of the increase in photocatalytic activity[18]. The extraction of zinc and divalent cadmium ions from wastewater used an adsorbent based on GO-TiO_2. The material removed 99.09% of zinc ions and 90.99% of cadmium ions under ideal conditions. The creation and utilization of GO-Silica, a decorated GO nanocomposite for the adsorptive removal of hazardous lead and mercury ions, is an important development in environmental remediation[9]. In this study, the synthesis of a $SrFe_{12}O_{19}/TiO_2/SiO_2/GO$ nanocomposite is presented. The morphology and composition of the nanocomposite were characterized using UV-DRS, XRD, SEM, VSM and EDAX techniques. Photocatalytic experiments were conducted to investigate the degradation of Rhodamine B and methylene blue dyes using the synthesized materials.

Material and Methods

The chemicals used to synthesize $SrFe_{12}O_{19}/TiO_2/SiO_2/GO$ nanocomposite are tetra ethyl ortho silicate, ethylene glycol, strontium nitrate, ferric citrate, citric acid, titanium tetra chloride, hydrochloric acid, phosphoric acid, potassium permanganate, hydrogen peroxide and Sulfuric acid. All chemicals used were of analytical grade and were utilized directly without further purification. Deionized water was employed in all the reactions.

Synthesis of Strontium Ferrite NPs: A strontium nitrate solution is created by dissolving 4.23 grams of strontium nitrate in 10 millilitres of distilled water. A solution of ferric citrate is prepared by dissolving 71.64 grams of ferric citrate in 10 milliliters of distilled water. The beaker contains a combination of the two mentioned solutions and 12.6 grams of citric acid are added to gradually lower the solution's pH neutrality by adding ammonia. Next, 20 milliliters of ethylene glycol are to be added. The solution is heated on a hot plate for two hours until a dry powder is obtained, following an 800^0 C calcination to produce fine strontium ferrite nanopowder.

Synthesis of TiO_2: In a beaker covered with aluminium foil, 350 ml of distilled water with 0.5 ml of HCl solution were gradually mixed with 6.9 g of $TiCl_4$. After an hour of magnetic stirring, the beaker produced a white, curdy precipitate. The mixture was heated to 80 to 100 °C on a hot plate. After obtaining the fine powder, moisture was removed by keeping it in a hot air oven set at 80 °C. Ultimately, the powder was ground in a motor pestle and calcined for two hours at 400°C[15].

Synthesis of SiO_2: A tetraethyl orthosilicate solution is prepared by mixing 0.3 moles of ethanol with TEOS. From 0.1 to 0.75 moles to prepare ammonia solution, add 0.25–2.0 moles of more ethanol together with ammonia. After drying at 80°C for six hours and calcining at 900°C for two hours, two solutions are combined and vigorously stirred for thirty minutes.

Synthesis of Graphene Oxide: A modified Hummers' method was employed to synthesize graphene oxide (GO)

from pure graphite powder. Initially, 27 milliliters of sulfuric acid (H_2SO_4) were mixed with 3 milliliters of phosphoric acid (H_3PO_4) in a 9:1 volume ratio and stirred for a few minutes. Then, 0.225 grams of powdered graphite were added to the mixture while continuing to stir. Following this, 1.32 grams of potassium permanganate ($KMnO_4$) were gradually incorporated into the mixture. After six hours of stirring, the solution turned dark green.

To remove excess $KMnO_4$, 0.675 milliliters of hydrogen peroxide (H_2O_2) were slowly added and the mixture was stirred for ten minutes. Following the exothermic reaction, the solution was allowed to cool. Finally, 30 milliliters of deionized water (DIW) and 10 milliliters of hydrochloric acid (HCl) were added[12].

Synthesis of $SrFe_{12}O_{19}/TiO_2/SiO_2$/GO nanocomposite: The process with GO and $SrFe_{12}o_{19}/TiO_2/SiO_2$ was used to synthesize the $SrFe_{12}O_{19}/TiO_2/SiO_2$/GO nanocomposites.To prepare the $SrFe_{12}o_{19}/TiO_2/SiO_2$-10% GO nanocomposites, one milliliter of 10 percent graphene oxide was detached in 20 mL of DI water in an ultrasonic cleaner for 30 minutes for sonication. Next, 1 gram of $SrFe_{12}O_{19}/TiO_2/SiO_2$ was dispersed in the prepared GO solution and sonicated for an additional 30 minutes. The resulting mixture was then continuously stirred for approximately 4 hours. The brown-colored product was gathered and dehydrated in a hot air oven for 2 hours at 80^0C.

Instrumentation: The produced nanocomposites were categorized using X-ray diffraction (XRD) to verify the virtue and crystallite size of the photocatalysts. This analysis was performed on a Bruker DX-5 progressive, equipped with a proportionate counter, using Cu Kα radiation (λ = 1.54 Å). Scanning electron microscope (SEM) images were obtained with a Carl Zeiss Gemini 300 of Germany. A transmission electron microscope (TEM) was utilized to control the shape and verify the particle size of the material. Fourier transform infrared (FTIR) spectroscopy was applied to examine the vibrational modes of the composite samples. The IR spectra of the samples were collected using an IR Prestige 21 spectrometer within the range of 500 to 4000 cm^{-1}. UV-Vis diffuse reflectance spectra were employed to analyze the structure and band gap of the composite, with the wavelength and absorbance measured using a UV DRS (Shimadzu 2600R) and $BaSO_4$ as a reference, covering the range of 200 to 800 nm. The magnetic properties of the photocatalyst composite were evaluated at room temperature using a vibrating sample magnetometer (VSM).

Results and Discussion

UV-Vis DRS analysis and band structure determination: The optical properties and the band gap energy of the as- fabricated $SrFe_{12}O_{19}$-TiO_2-SiO_2-GO were examined using UV-Vis diffuse reflectance spectroscopy (DRS). At 450 nm, the sample exhibits distinct absorptions. The presence of an absorption maximum at 450 nm confirms the formation of the hexagonal phase, indicating a well-defined crystalline lattice structure. The DRS data, along with the Kubelka–Munk (K–M) model, was used to evaluate the bandgap energy (BE) of the fabricated samples based on their spectral data, as shown in fig. 1. The estimated bandgap energy for the $SrFe_{12}O_{19}$–TiO_2–SiO_2–GO sample is 2.29eV. The band gap value is less than 3eV, indicating high efficiency in utilizing solar energy and the potential for photocatalysis.

X-ray diffraction studies: The $SrFe_{12}O_{19}$–TiO_2–SiO_2–GO nanocomposite as a photocatalyst is shown by the X-ray diffraction (XRD) pattern in figure 2.

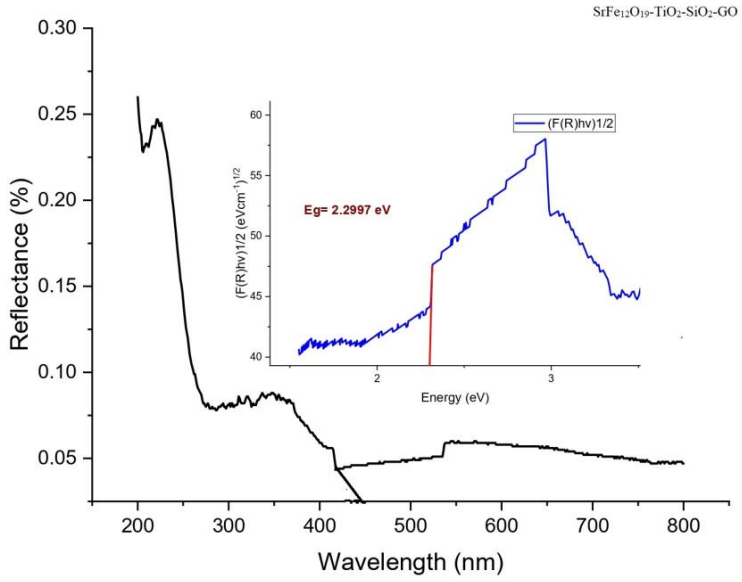

Fig. 1: UV-Visible diffuse reflectance spectra of $SrFe_{12}O_{19}$ / TiO_2/SiO_2 /GO

The average crystallite size (D) and the most intense diffraction peaks spotted experimentally were matched and indexed using JCPDS Card Nos. 84-1531, 021-1272 and 00-041-148710 for $SrFe_{12}O_{19}$, TiO_2 and GO in the anatase and spinel phases correspondingly. As seen in figure 2, sharp and intense peaks for the GO-$SrFe_{12}O_{19}$ component are observed at 2θ values of 10°, 25°, 34°, 35°, 55° and 57°, corresponding to the planes (001), (101), (107), (114), (105) and (2011). The XRD planes (001), (107), (114) and (2011) confirm that GO and $SrFe_{12}O_{19}$ are the primary phases, highlighting the crystalline nature of the sample.

Due to its amorphous nature, the SiO_2 peak is not observed, while the peaks at 2θ values of 25° and 55° for the TiO_2 photocatalyst correspond to the (101) and (105) planes, together with the peaks and planes of $SrFe_{12}O_{19}$, TiO_2 and GO in the XRD pattern. The crystallite sizes of $SrFe_{12}O_{19}$, SiO_2, TiO_2 and GO were determined using the Scherrer formula. The analysis confirms that the composite sample was successfully formed, with strontium ferrite exhibiting a cubic spinel structure existing in the anatase crystalline phase of TiO_2.

FTIR: The examined samples' FT-IR spectra are shown in fig. 3. The primary bands at 3848–2355 cm^{-1} are the vibrations of hydroxyl groups (the hydrogen-bonded –OH···H at 3677 cm^{-1}, the isolated –OH in TiO_2 and, or $Srfe_{12}O_{19}$ at 3789 cm^{-1} and the isolated silanol groups ≡SiOH at 3789 cm^{-1}). The sample with the highest band intensity among the SiO_2-containing samples' spectra has isolated –OH groups.

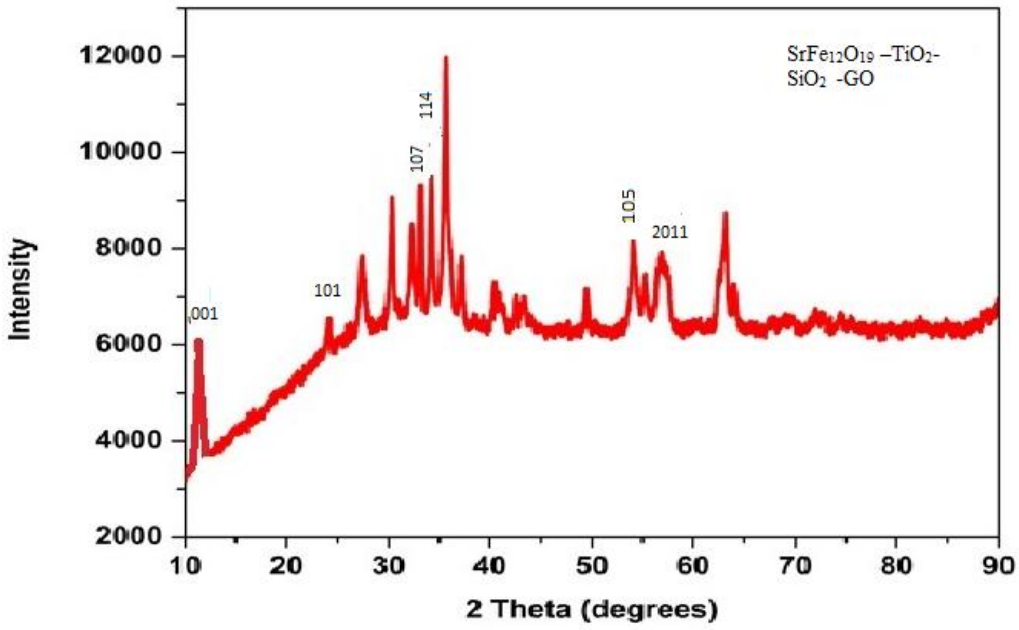

Fig. 2: XRD pattern of $SrFe_{12}O_{19}$/ TiO_2/SiO_2 /GO

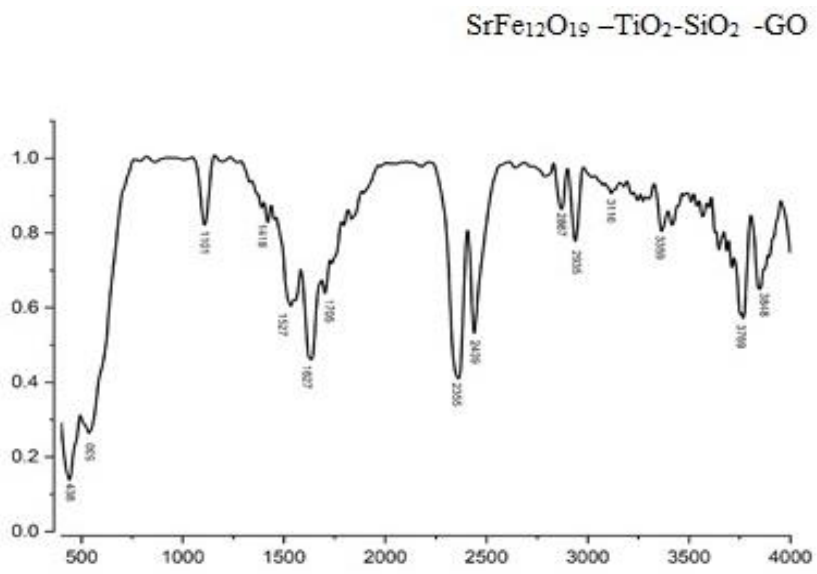

Fig. 3: FTIR of $SrFe_{12}O_{19}$/ TiO_2/SiO_2 /GO

The samples lacking silica do not exhibit those bands; on the other hand, the samples with TiO_2 and $SrFe_{12}O_{19}$ exhibit bands of isolated hydroxyl groups that shift towards lower wavenumbers (3677 cm^{-1}). The presence of hydrogen-bonded SiOH–OSi groups, or more specifically, the presence of internal hydroxyl groups, is caused by peaks with a maximum at~3677 cm^{-1}. The existence of hydrogen-bonded SiOH-OSi groups, or more specifically, the occurrence of internal hydroxyl groups, is caused by the peaks with a maximum at~3677 cm^{-1}. The wideband, which peaks at around 3359 cm^{-1}, exhibits physically adsorbed water and –OH and hydrogen-bonded –OH···H in the oxide structures. The silica-containing samples' spectra show that the asymmetric stretching vibrations of Si–O–Si bridges are responsible for the broad, intense bands in the range of 1418–1101 cm^{-1}, while the symmetric stretching and deformation modes of Si–O–Si are attributed to the peaks at ~530 cm^{-1} and ~470 cm^{-1}, respectively. The observed band at 1720 cm^{-1} was assigned to the carboxyl group, a broad peak appeared at 3359 cm^{-1} in the highest frequency attributed to the stretching mode of O-H bond.

SEM and EDS: To examine the structural morphology of the $SrFe_{12}O_{19}$–TiO_2–SiO_2–GO photocatalysts and nanocomposite by SEM, figure 4 shows the SEM images, revealing exclusively spherical nanoparticles. However, a significant degree of aggregation and varying surface morphologies were noticed in the $SrFe_{12}O_{19}$–SiO_2 sample, likely because of the magnetic attraction between the strontium ferrite and silica layers. The $SrFe_{12}O_{19}$–TiO_2–SiO_2–GO sample displays a heterogeneous structure with a high degree of surface roughness, a feature not detected in the pristine TiO_2 photocatalyst. The image also indicates the presence of spherical-shaped nanoparticles and some TiO_2 aggregates, resulting from the hydrolysis of titanium dioxide. Figure 4 also presents the energy-dispersive X-ray spectroscopy (EDS) spectrum of the $SrFe_{12}O_{19}$/SiO_2/ TiO_2/GO nanostructures, confirming the presence of Sr, Si, Fe, O, C and Ti elements. These results suggest that the sample precursors were set as projected, circuitously confirming the establishment of the composite.

TEM: The characterization of $SrFe_{12}O_{19}$-TiO_2-SiO_2-GO (Strontium hexaferrite, Titanium dioxide, Silicon dioxide and Graphene oxide) nanocomposites using Transmission Electron Microscopy (TEM) offers complete perception into the structural, morphological and compositional aspects of the material. TEM can reveal the size and shape of the $SrFe_{12}O_{19}$, TiO_2 and SiO_2 nanoparticles within the composite. This helps in understanding the distribution and uniformity of the particles, which is crucial for the material's magnetic and photocatalytic properties. The presence and morphology of graphene oxide sheets in the composite can be observed including their thickness, lateral dimensions and how they interact with the other nanoparticles. High-resolution TEM (HRTEM) can be used to identify the crystalline structure of the $SrFe_{12}O_{19}$, TiO_2 and SiO_2 phases. Lattice fringes observed in HRTEM images help in determining the crystallographic orientation and identifying any lattice defects.

The interface between the different components ($SrFe_{12}O_{19}$, TiO_2, SiO_2 and GO) can be examined to understand the bonding and interaction at the nanoscale. This is important for understanding how the composite materials integrate at the atomic level. TEM can provide insights into how well the different components of the nanocomposite are bonded at the nanoscale. Strong interfacial bonding is essential for enhancing the composite's mechanical strength, magnetic properties and overall stability..TEM characterization of the $SrFe_{12}O_{19}$-TiO_2-SiO_2-GO composite provides a comprehensive understanding of the material's structure at the nanoscale, which is vital for tailoring its properties for specific applications like magnetic data storage, catalysis, or electromagnetic interference shielding.

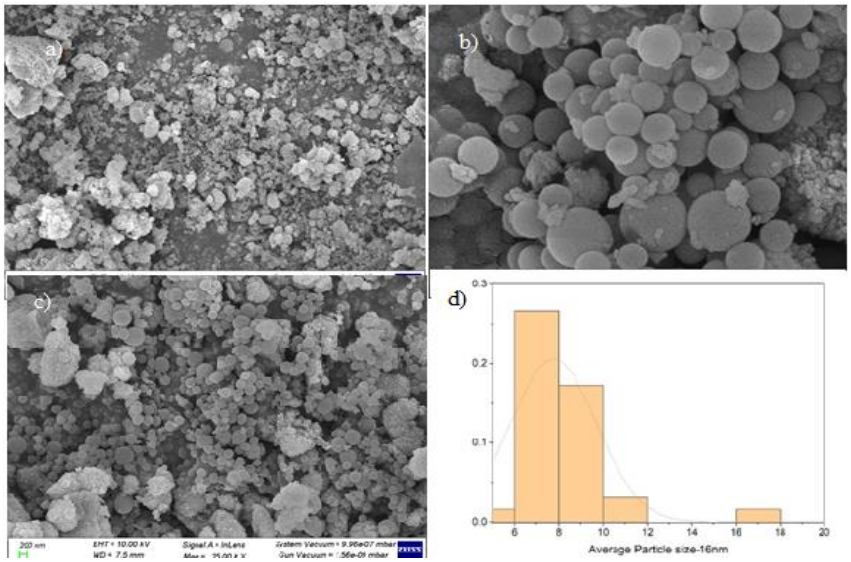

Fig. 4: SEM images of $SrFe_{12}O_{19}$/ TiO_2/SiO_2 /GO a)1µm b)100nm c)200nm d) Particle size distribution of $SrFe_{12}O_{19}$/ TiO_2/SiO_2 /GO

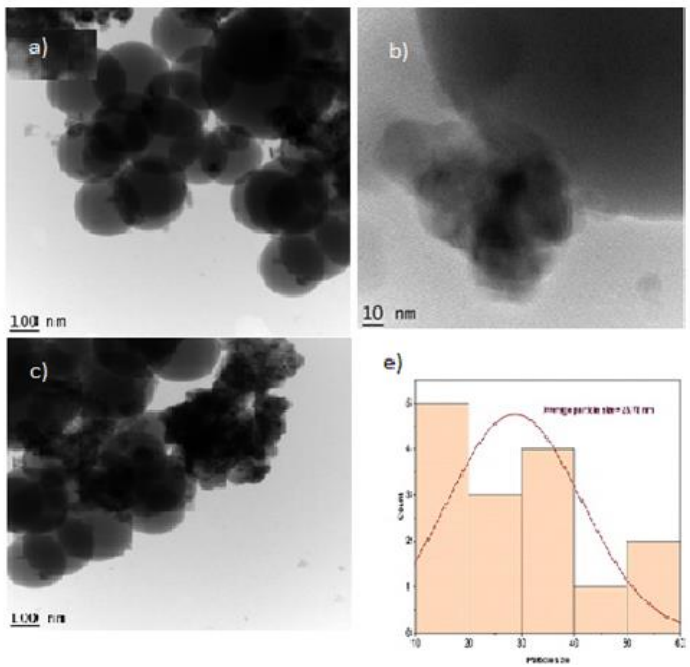

Fig. 5: TEM images of $SrFe_{12}O_{19}$/ TiO_2/SiO_2 /GO a) 100nm b) 10nm c) 100nm d) Particle size distribution of $SrFe_{12}O_{19}$/ TiO_2/SiO_2 /GO

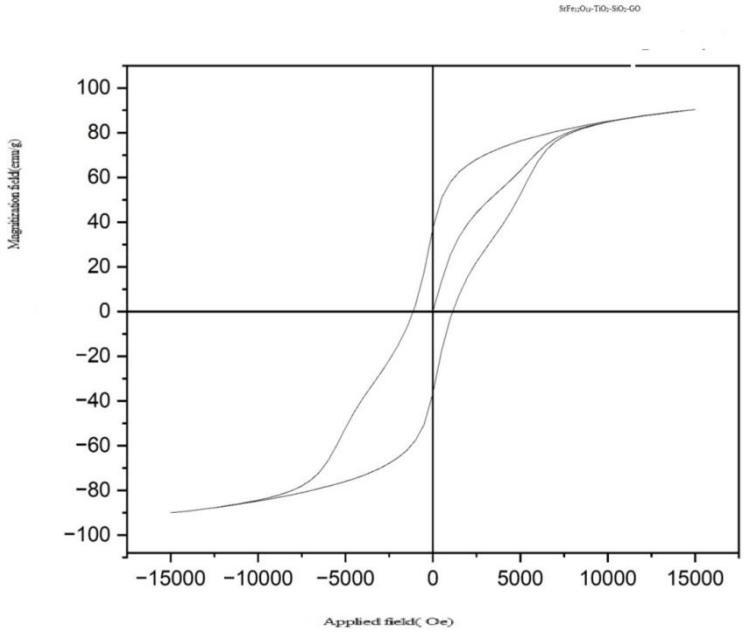

Fig. 6: Magnetization loop for $SrFe_{12}o_{19}$/TiO_2/SiO_2/GO composite at room temperature

VSM: The samples magnetic property was examined using a vibrating sample magnetometer(VSM) system at normal temperature. Hysteresis loop of magnetic $SrFe_{12}O_{19}$ –TiO_2-SiO_2 –GO nanoparticles was prepared by Sol-Gel and Hummers method. Synthesized nanoparticles display superparamagnetic behavior, with a saturation magnetization of 80 emu/g and a coercivity that tends towards zero Oe. The nanoparticles exhibit adequate magnetization for magnetic recycling, making them suitable for use as the core of a recyclable photocatalyst.

The hysteresis loop of magnetic $SrFe_{12}O_{19}$ –TiO_2-SiO_2 –GO nanoparticles is portrayed. The result also demonstrates superparamagnetic behavior and exhibits a saturation magnetization of 80 emu/g indicating that bulk magnetite is utilized as a catalyst for environmental applications, with a coercivity of approximately zero Oe. This magnetization indicates that $SrFe_{12}O_{19}$ –TiO_2-SiO_2 –GO composite inherits the magnetic property from the $SrFe_{12}O_{19}$. The vital characteristics of magnetic property of the prepared nanocomposites is re-generable and re-usable magnetic heterogeneous catalyst.

Photocatalytic activity

The synthesized sample of photocatalytic activity was evaluated by degrading Rhodamine B and Methylene blue in

aqueous solutions. A 300W Xenon lamp, which emits a broad spectrum of UV and visible light, served as the light source. To specifically investigate photocatalytic activities under visible light, the light was filtered through glass to block wavelengths shorter than 400 nm. The photocatalytic reactions were carried out in a 200 ml reactor (40 mm height, 85 mm) with stirring. The STSG photocatalyst was used to degrade Rhodamine B and MB. The initial concentrations of the Rhodamine B and MB solutions were 10.0 mg/l. During the photocatalytic investigations, the Rhodamine B and MB solutions containing the photocatalyst were stirred in the dark to allow adsorption/desorption equilibrium until the concentrations stabilized. Following irradiation, each 5.0 ml samples of the dispersion was centrifuged to separate the photocatalyst and the supernatant was analyzed using a UV-Vis spectrophotometer at a wavelength of 461.7 nm.

Effect of Initial Dye Concentration: The degradation percentage and initial dye concentration are depicted in fig. 7a and 7b. The impact of the initial dye concentration was studied by increasing the concentration of Rh B and MB, ranging from 5ppm to 100ppm. Both dyes degradation percentage dropped gradually. Rh B shows 100% degradation at 120min and MB dye at 125 min for dye concentration 10 ppm. The main reason for dye degradation is the decrease in OH- production at this stage, which leads to a reduced absorption capacity of the catalyst as the dye concentration increases.

Effect of pH: The photocatalytic degradation of Rh B and MB onto $SrFe_{12}O_{19}$-TiO2-SiO2-GO is studied at pH range 2 to 11, with a dye concentration of 10 ppm of composite and an irradiation period of 120 minutes. The efficiency of $SrFe_{12}O_{19}$-TiO_2-SiO_2-GO degradation is primarily determined by the pH of the solution. For both dyes, the degradation percentage is 100% at pH 7 for MB, while for Rh B it is at pH 8 at different time intervals (100 min,90min). When the pH rises from 4 to 8, the solution contains more negative-charged photocatalysts that can generate more hydroxyl radicals Ti-OH is stable at this pH, which means the photocatalyst functions best at capturing the right amount of energy to make the photocatalytic process effective. Several researchers have observed similar results when using modified composites as a photocatalyst in the dye removal process. From the result, it may be concluded that $SrFe_{12}O_{19}$-TiO_2-SiO_2-GO can be used as an effective photocatalyst to degrade Rh B than MB.

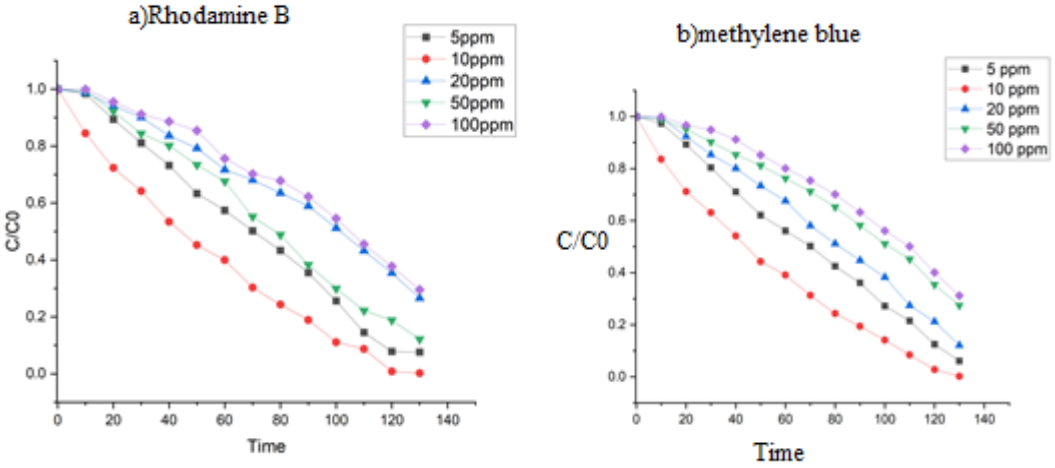

Fig. 7: Effect of initial dye concentration on the photocatalytic degradation of Rh B and MB dyes

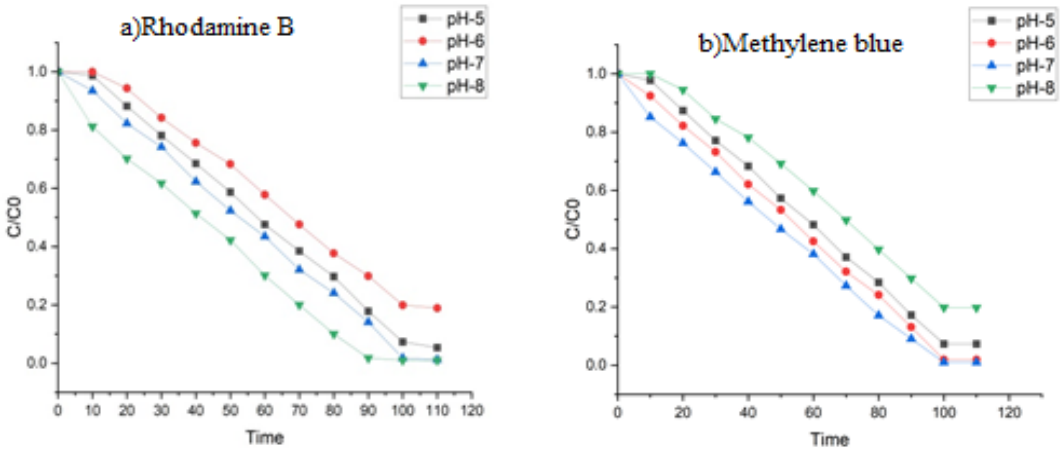

Fig. 8: Effect of pH on the photocatalytic degradation of Rh B and MB dyes

Effect of Temperature: Current research indicates that environmental temperature significantly affects photodegradation. The temperature effect of Rh B and MB onto $SrFe_{12}O_{19}$-TiO2-SiO2-GO is studied at pH-7, with a dye concentration of 10 ppm of composite and an irradiation period of 120 minutes. By raising the temperature from 30^0C to 45^0C, the photocatalytic efficiency can rise approximately two to three times. Since UV light is a component of solar energy, it can initiate the photocatalytic process and raise the temperature of the photocatalytic system. The results of the research demonstrated that they cannot be pyrolyzed by heating to a temperature below 45^0C or self-degrade by absorbing radiation. The Rh B degraded 100% at 80min and MB degraded at 90min The effective degradation was achieved when both $SrFe_{12}O_{19}/SiO_2/TiO_2$/GO and UV radiation were applied. $SrFe_{12}O_{19}/TiO_2/SiO_2$/GO nanocomposite is useful photocatalysts and Rh B is more efficient dye than MB.

Effect of catalyst dose: The degradation efficiency of Methylene Blue (MB) and Rhodamine B (Rh B) using the $SrFe_{12}O_{19}$-TiO_2-SiO_2-GO composite was evaluated at pH 7, with a dye concentration of 10 ppm of composite, temperature at 35^0C and an irradiation period of 120 minutes varying the amount of the composite from 0.20 to 0.50 g/l under optimal conditions. The relationship between the catalyst dosage and C/C_0 for MB and Rh B is illustrated. As shown, the degradation percentage increases progressively with the catalyst dose up to 0.40 g/l when the dye solution concentration is low. The maximum degradation was achieved at 100% for Rh B at 50min and for MB at 55min. Beyond this dosage, there is no significant improvement in degradation efficiency for either dye. This plateau may be due to the formation of a cloudy, opaque solution resulting from the excessive addition of the catalyst.

Irradiation time: It should be noted that exposure to visible light can photoexcite Rh B, the model pollutant. To rule out the potential impact of the dye on the assessment of the materials' catalytic activity, we also conducted photodegradation tests using several dyes such as Methylene blue (MB) and Rhodamine B (Rh B), under identical conditions. The absorbance fluctuation of the RhB and MB solutions under visible light at various irradiation times is displayed.

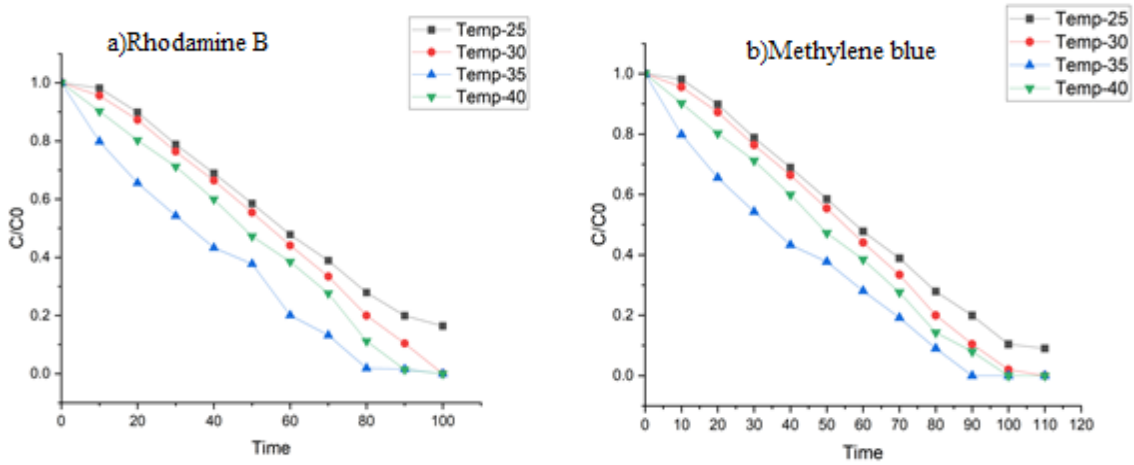

Fig. 9: Effect of temperature on the photocatalytic degradation of Rh B and MB dyes

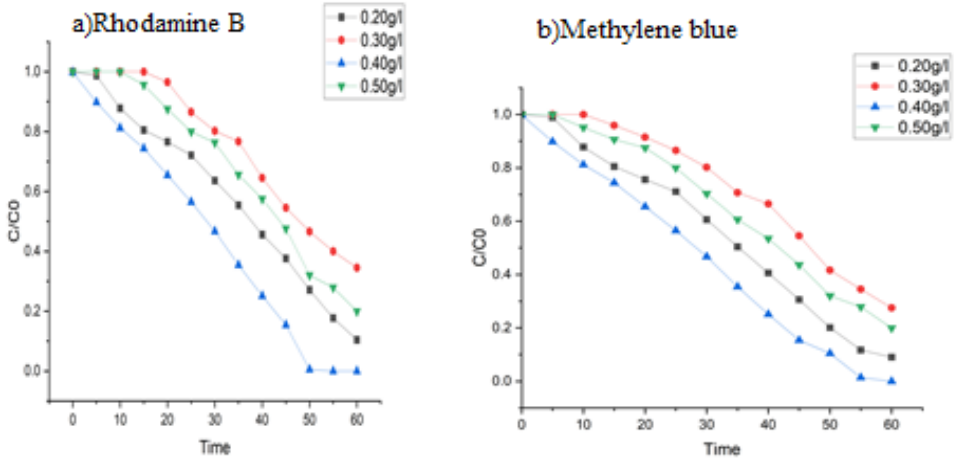

Fig. 10: Effect of catalyst dosage on the photocatalytic degradation of Rh B and MB dyes

During the illumination time, the absorption peaks of RhB and MB noticeably diminish and nearly vanish after 50 and 55 minutes respectively. The ferrite-coated TiO_2 was generated at pH = 8, catalyst load 0.40g/l and temperature 35^0C is an excellent semiconducting photocatalytic material with a unique universal advantage to degrade several dyes, including MB and RhB.

Stability and reusability: To evaluate the stability and reusability of the $SrFe_{12}O_{19}$-TiO_2-SiO_2-GO heterojunction, cycling experiments were performed for the photodegradation of RhB under visible light. After three additional cycles, the degradation efficiency showed a slight decline from 80 to 70%, likely due to photo-bleaching on the $SrFe_{12}O_{19}$-TiO_2-SiO_2-GO surface.

However, the XRD pattern of the heterojunction after these photocatalytic reactions demonstrates that its phase and structure remain unchanged. These results indicate that the nanocomposite heterojunction photocatalyst is stable and retains its activity during the photodegradation of the organic dye.

Antibacterial activity: Utilising the technique of disc diffusion, the antibacterial activity of particular $SrFe_{12}O_{19}$-TiO_2-SiO_2-GO materials has been evaluated and compared to the commercial antibiotic Cefalexin. Muller Hinton agar composition was examined using the disc diffusion method in (g/L). Three concentrations of 10, 20 and 30 mg/ml were employed to evaluate the antibacterial activity of the substances against Gram-positive and Gram-negative *Staphylococcus pneumonia* and *Klebsella*, accordingly. Particle size influences $SrFe_{12}O_{19}$-TiO_2-SiO_2-GO's antibacterial activity.

Both Gram-positive and Gram-negative bacteria do not exhibit any antibacterial action against $SrFe_{12}O_{19}$-TiO_2-SiO_2-GO (0). All other $SrFe_{12}O_{19}$-TiO_2-SiO_2-GO composites, on the other hand, have antibacterial properties. Table 1 provided the ferrite content, the percentage of optimum metal oxide precursor and the appropriate zone of inhibition value. This is centred, as stated, on the structural differences between bacteria that are Gram-positive and those that are Gram-negative.

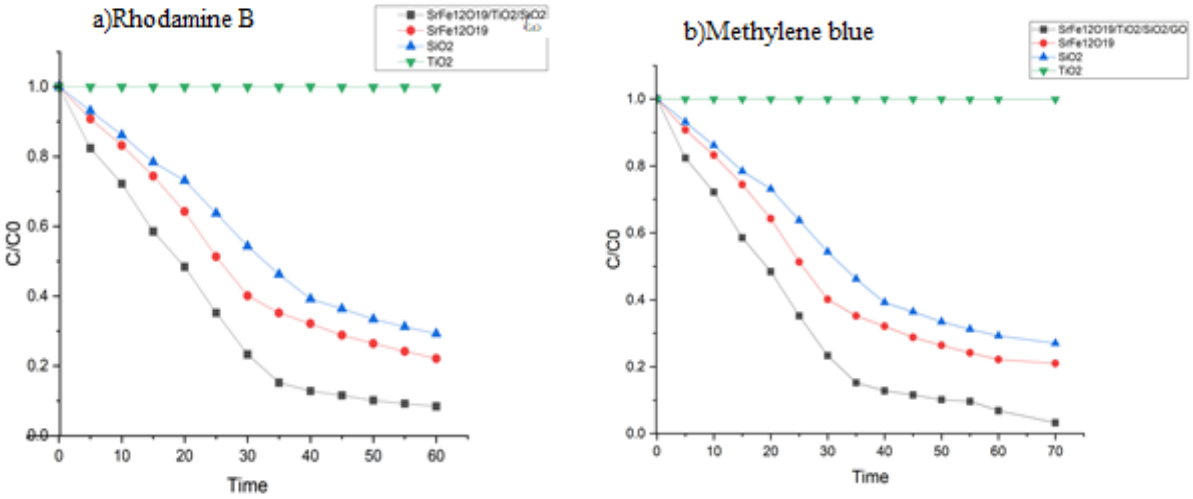

Fig. 11: Effect of irradiation time on the photocatalytic degradation of Rh B and MB dye

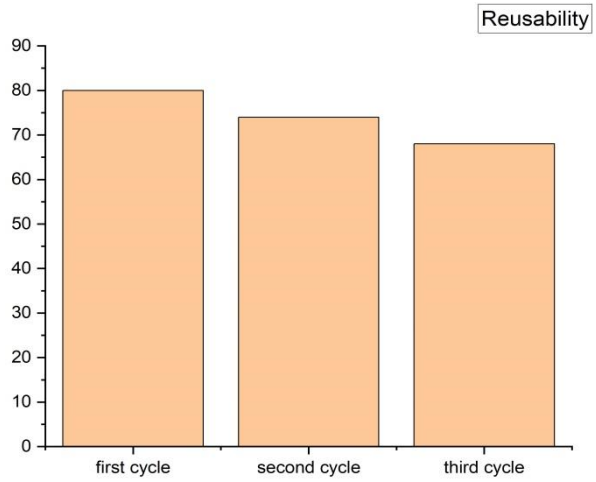

Fig. 12: Stability and reusability of $SrFe_{12}O_{19}$-TiO_2-SiO_2-GO

Table 1
Antibacterial activity of $SrFe_{12}O_{19}$-TiO_2-SiO_2-GO

S.N.	Sample	Concentration(µg/ml)	*Staphylococcus pneumonia* (Gram positive) mm	*Klebsella* (Gram negative) mm
A	$SrFe_{12}O_{19}$-TiO_2-SiO_2-GO synthesized	10	3	3
		20	3	4
		30	3	3
	Cefalexin	10	19	22
B	$SrFe_{12}O_{19}$-TiO_2-SiO_2-GO nanocomposite/ Cefalexin	10	15	14
		20	16	18
		30	18	19
	Cefalexin	10	20	23

The results show that when the proportion is increased from 10 to 30, the antibacterial activities also increase. Reactive oxygen species like O_2^{-2}, H_2O_2 and HO• are said to be the cause of the degradation mechanism, which leads to protein oxidation, nucleic acid breakdown and disruption of metabolic processes.

The NPs' smaller size, which allows for better surface interaction with bacteria and cell membrane penetration, is the cause of their increased antibacterial activity. Furthermore, the accumulation of nanocomposite in the periplasmic /cytoplasmic area and their deposition on the surface have been identified as a mechanism of distraction leading to bacterial mortality. However, the release these ions could be harmful if released. The lack of any band position shift on $SrFe_{12}O_{19}$-TiO_2-SiO_2-GO, as confirmed by O_2^{-2} on the XRD pattern, would suggest that there is no structural distortion caused by the inclusion of Fe^{3+} or Mn^{3+} ions. It might also foreshadow the remarkable solubility and stability of these metal oxides in water.

Conclusion

The work presents the nanocomposite magnetic photocatalyst. The $SrFe_{12}O_{19}$-TiO_2-SiO_2-GO nanocomposite was synthesized using the sol-gel and Hummers methods. Its photocatalytic activity was tested using Rh B and MB under UV-Vis light irradiation. The characterization results obtained through UV-DRS, XRD, FTIR, SEM, TEM and VSM indicate that $SrFe_{12}O_{19}$-TiO_2-SiO_2-GO is a good photocatalyst and a reusable, easily separable magnetic composite.

Acknowledgement

The authors are thankful to authorities of Andhra university for offering the research facilities and the Advanced Analytical Laboratory, Andhra university, Visakhapatanam, India for providing the spectral analysis.

References

1. Abdullah Khaled Al-Buriahi, Adel Ali Al-Gheethi, Ponnusamy Senthil Kumar, Radin Maya Saphira Radin Mohamed, Hanita Yusof, Abdullah Faisal Alshalif and Nasradeen A. Khalifa, Elimination of rhodamine B from textile wastewater using nanoparticle photocatalysts: A review for sustainable approaches, *Chemosphere*, **287**, 132162 **(2022)**

2. Ahmad S.Z.N., Salleh W.N.W., Ismail A.F., Yusof N., Yusop M.Z.M. and Aziz F., Adsorptive removal of heavy metal ions using graphene-based nanomaterials: toxicity, roles of functional groups and mechanisms, *Chemosphere*, **248**, doi:10.1016 /j.chemosphere.2020.126008 **(2020)**

3. Azrina Abd Aziz, Yeu Harng Yau, Gianluca Li Puma, Carolin Fischer, Shaliza Ibrahim and Saravanan Pichiah, Highly efficient magnetically separable TiO_2–graphene oxide supported SrFe12O19 for direct sunlight-driven photoactivity, *Chemical Engineering Journal*, **235**, 264 – 274 **(2014)**

4. Chengyun Zhao, Mengyao Shen, Zhenxing Li, Rui Sun, Ailin Xia anb Xianguo Liu, Green synthesis and enhanced microwave absorption property of reduced graphene oxide-SrFe12O19 nanocomposites, *Journal of Alloys and Compounds*, DOI: 10.1016/j.jallcom.2016.08.078 **(2016)**

5. Elaiyappillai Elanthamilan, I. Betsy Elizabeth, Sea-Fue Wang and I. Sharmila Lydia, Strontium hexaferrite microspheres: Synthesis, characterization and visible-light-driven photocatalytic activity towards the degradation of methylene blue dye, *Optical Materials*, **137**, 113565 **(2023)**

6. Fatemeh Bavarsiha, Masoud Rajabi and Mehdi Montazeri-Pour, Synthesis of $SrFe1_2O_{19}$/SiO_2/TiO_2 composites with core/shell/shell nanostructure and evaluation of their photocatalytic efficiency for degradation of methylene blue, *J Mater Sci: Mater Electron*, DOI: 10.1007/s10854-017-8098-5 **(2017)**

7. Hesham Hamad et al, Synthesis and characterization of core–shell– shell magnetic (CoFe2O4–SiO2–TiO2) nanocomposites and TiO_2 nanoparticles for the evaluation of photocatalytic activity under UV and visible irradiation, *New Journal of Chemistry*, **39**, 3116-3128 **(2015)**

8. Jain Rajeev, Mathur Megha, Sikarwar Shalini and Mittal Alok, Removal of the hazardous dye rhodamine B through photocatalytic and adsorption treatments, *Journal of Nanomaterials*, **85(4)**, 956-964 **(2017)**

9. Jayakaran Pachiyappan and Nirmala Gnanasundaram, Using graphene oxide-silica [go-si] nano composite adsorbent, removal

of heavy metal ions (lead and mercury) from industrial wastewater and analysing its performance, *RJC*, **13**, 2028 **(2020)**

10. Joshi Naveen Chandra and Gururani Prateek, Advances of graphene oxide based nanocomposite materials in the treatment of wastewater containing heavy metal ions and dyes, *Current Research in Green and Sustainable Chemistry*, **5**, 100306 **(2022)**

11. Masomeh Taghipour, Mohammad Yousefi, Reza Fazaeli and Masoud Darvish Ganji, Variable band-gap Sr-hexagonal ferrites on carboxylated graphene oxide composite as an efficient photocatalytic semiconductor, *J. Nanoanalysi*, **9(3)**, 193-205 **(2022)**

12. Medidi Sunitha et al, Photocatalytic Degradation of Methylene Blue and Malachite Green Dyes with CuWO 4 -GO Nano Composite, *Modern Research in Catalysis*, **7(2)**, 17-34 **(2018)**

13. Mouhsine Laayati, Ayoub Abdelkader Mekkaoui, Lahcen Fkhar, Mustapha Ait Ali, Hafid Anane, Lahoucine Bahsis, Larbi El Firdoussi and Soufiane El Houssam, Synergistic effect of GO/SrFe12O19 as magnetic hybrid nanocatalyst for regioselective ring-opening of epoxides with amines under eco-friendly conditions, *RSC Adv*., https://doi.org/10.1039/D2RA00984F **(2022)**

14. Peralta Marcos E., Ocampo Santiago, Funes Israel G., Medina Florencia Onaga, Parolo María E. and Carlos Luciano, Nanomaterials with Tailored Magnetic Properties as Adsorbents of Organic Pollutants from Wastewaters, *Inorganics*, **8(4)**, 24 **(2020)**

15. Shumaila Rafaqat, Naeem Ali, Cesar Torres and Bruce Rittmann, Recent progress in the treatment of dyes wastewater using microbial-electro-Fenton technology, *RSC Adv*, **12(1)**, 17104-17137 **(2022)**

16. Somasekhar Ryali and Paul Douglas Sanasi, Graphene oxide–nano-titania composites for efficient photocatalytic degradation of indigo carmine, *Journal of the Chinese Chemical Society*, **65**, 1423 **(2018)**

17. Trang Nguyen Thi Quynh, Ngoc Ngo Quy Thao, Long Dang Thanh and Thanh Pham, Antioxidant and Antibacterial activity of Lotus tea in Thua Thien Hue province from Vietnam, *Res. J. Biotech.*, **18(12)**, 48-54 **(2023)**

18. Zuzanna Bielan, Agnieszka Sulowska, Szymon Dudziak, Katarzyna Siuzdak, Katarzyna Siuzdak and Anna Zielińska-Jurek, Defective TiO_2 Core-Shell Magnetic Photocatalyst Modified with Plasmonic Nanoparticles for Visible Light- Induced Photocatalytic Activity, *Catalysts*, **10(6)**, 672 **(2020)**.

(Received 17th September 2024, accepted 20th November 2024)